\

Topological phases and type-II edge state in two-leg-coupled Su-Schrieffer-Heeger chains

Tianqi Luo(罗天琦), Xin Guan(关欣), Jingtao Fan(樊景涛), Gang Chen(陈刚), and Suo-Tang Jia(贾锁堂)

What follows is a list of articles you may be interested in

Tunable optomechanically induced transparency and fast-slow light in a loop-coupled optomechanical system

Qinghong Liao(廖庆洪), Xiaoqian Wang(王晓倩), Gaoqian He(何高倩), and Liangtao Zhou(周良涛)

Controllable four-wave mixing response in a dual-cavity hybrid optomechanical system

Lei Shang(尚蕾), Bin Chen(陈彬), Li-Li Xing(邢丽丽), Jian-Bin Chen(陈建宾), Hai-Bin Xue(薛海斌), and Kang-Xian Guo(郭康贤)

Quantum plasmon enhanced nonlinear wave mixing in graphene nanoflakes

Hanying Deng(邓寒英), Changming Huang(黄长明), Yingji He(何影记), and Fangwei Ye(叶芳伟)

Realization of adiabatic and diabatic CZ gates in superconducting qubits coupled with a tunable coupler

Huikai Xu(徐晖凯), Weiyang Liu(刘伟洋), Zhiyuan Li(李志远), Jiaxiu Han(韩佳秀), Jingning Zhang(张静宁), Kehuan Linghu(令狐克寰), Yongchao Li(李永超), Mo Chen(陈墨), Zhen Yang(杨真), Junhua Wang(王骏华), Teng Ma(马腾), Guangming Xue(薛光明), Yirong Jin(金贻荣), and Haifeng Yu(于海峰)

Phase-sensitive Landau-Zener-Stückelberg interference in superconducting quantum circuit

Zhi-Xuan Yang(杨智璇), Yi-Meng Zhang(张一萌), Yu-Xuan Zhou(周宇轩), Li-Bo Zhang(张礼博), Fei Yan(燕飞), Song Liu(刘松), Yuan Xu(徐源), and Jian Li(李剑)

Topological phases and type-II edge state in two-leg-coupled Su–Schrieffer–Heeger chains

Tianqi Luo(罗天琦)[1,2], Xin Guan(关欣)[3,†], Jingtao Fan(樊景涛)[1,2,‡],
Gang Chen(陈刚)[1,2,4], and Suo-Tang Jia(贾锁堂)[1,2]

[1]*State Key Laboratory of Quantum Optics and Quantum Optics Devices, Institute of Laser Spectroscopy,
Shanxi University, Taiyuan 030006, China*
[2]*Collaborative Innovation Center of Extreme Optics, Shanxi University, Taiyuan 030006, China*
[3]*Taiyuan Institute, Taiyuan University, Taiyuan 030006, China*
[4]*Collaborative Innovation Center of Light Manipulations and Applications,
Shandong Normal University, Jinan 250358, China*

Topological quantum states have attracted great attention both theoretically and experimentally. Here, we show that the momentum-space lattice allows us to couple two Su–Schrieffer–Heeger (SSH) chains with opposite dimerizations and staggered interleg hoppings. The coupled SSH chain is a four-band model which has sublattice symmetry similar to the SSH4. Interestingly, the topological edge states occupy two sublattices at the same time, which can be regarded as a one-dimension analogue of the type-II corner state. The analytical expressions of the edge states are also obtained by solving the eigenequations. Finally, we provide a possible experimental scheme to detect the topological winding number and corresponding edge states.

1. Introduction

Since the topological aspect of the quantum Hall effect is revealed,[1–3] a phase transition mechanism beyond Ginzburg–Landau paradigm is being gradually established. Topological quantum states have attracted great attention due to their robustness against various disorders. Lots of topological phenomena have been explored, such as topological insulators (TIs),[4–8] topological semimetals,[9–12] high-order TIs,[13–15] topological Anderson insulators,[16–18] and non-Hermitian skin effect.[19–22] Many of these phenomena have been observed through different platforms, such as cold atom,[23–25] solid,[26,27] photonic crystal,[28,29] phononic crystal,[30–33] and superconducting circuits.[34–36]

Momentum-space lattice provides a powerful tool to study various interesting physical phenomena. It has been shown that two different mechanisms, a quantum version[37] and a classical version,[38] can be used to achieve the momentum-space lattice. The quantum one applies the so-called superradiance lattice,[39–41] in which the optical field couples different spin-wave states, known as timed-Dicke states,[42] to form a tight-binding model, by switching the phase-correlation wave vector discretely. The other mechanism, namely, the classical version, utilizes the classical interaction between light field and atoms. Under this paradigm, the recoil momentum of atoms becomes discrete, which offers opportunity to simulate lattice sites in solid systems.[43–45] The

latter owns a unique advantage that the boundaries of the lattices can be unambiguously determined. As such, it is preferable to use the classical version when focusing on physics confined on edges.

In this paper, we propose a two-leg-coupled Su–Schrieffer–Heeger (SSH) model by using the classical momentum-space lattice. By calculating the energy band and winding number, we obtain the topological phase diagram. It is found that the topological edge states occupy two sublattices at the same time, which can be regarded as a one-dimension analogue of the type-II corner state.[46] Then, we further demonstrate the existence of the type-II edge state by solving the eigenequations. Finally, the experimental schemes for the topological winding number and corresponding edge states detections based on current experimental setups are proposed.

2. Model and Hamiltonian

We consider a system of two-level ultracold atoms interacting with Bragg laser beams as shown in Fig. 1. Two of these lasers propagate rightward and carry wave numbers k_1 and k_2 (k_1/k_2 is irrational), respectively. The lasers propagating leftward can be sorted as two classes: the beams with wave number k_1 and the others with wave number k_2. The leftward propagating lasers characterized by k_1 (k_2) are composed of

---

$2(N-1)$ (N) discrete frequency components. After adiabatically eliminating the excited state, the momenta of atoms are shown to take quantized values $p_{m,n} = 2\hbar(mk_1 + nk_2)$, where m and n are integers (see Appendix A for details). Properly engineering the frequencies of the Bragg lasers such that the two-photon detuning with $w_1^+ - w_{1i}^- = (E_{m,n} - E_{m+1,n})/\hbar$ [$w_2^+ - w_{2i}^- = (E_{m,n} - E_{m,n+1})/\hbar$] is achieved, we are able to couple the momentum states $|n,m\rangle$ with $|n,m+1\rangle$ ($|n+1,m\rangle$). Here $E_{m,n} = (2m\hbar k_1 + 2n\hbar k_2)^2/2M$, and w_j^+ (w_{ji}^-) denotes the frequency of the laser beam propagating rightward (leftward) with wave number k_j, and the subscript i in w_{ji}^- specifies the i-th frequency component. After a rotating wave approximation,[38,43] the Hamiltonian is written as

$$
\begin{aligned}
\hat{H} = {} & \hbar \sum_{m,n} (\widetilde{\Omega}_{k_1,n+2m} |n,2m+1\rangle \langle n,2m| \\
& + \widetilde{\Omega}_{k_1,n+2m-1} |n,2m\rangle \langle n,2m-1|) \\
& + \hbar \sum_m (\widetilde{\Omega}_{k_2,2m} |1,2m\rangle \langle 0,2m| \\
& + \widetilde{\Omega}_{k_2,2m-1} |1,2m-1\rangle \langle 0,2m-1|) + \text{H.c.}, \quad (1)
\end{aligned}
$$

where $\widetilde{\Omega}_{l,i} = \Omega_{l,i}^- \Omega_l^+/4\Delta$, and $\Omega_{l,i}$ is the Rabi frequency of the light field with wave number l ($= k_1, k_2$) and frequency component i. By setting $\widetilde{\Omega}_{k_2,2m} = t_2$, $\widetilde{\Omega}_{k_2,2m-1} = t_1$, $\widetilde{\Omega}_{k_1,2m} = w$, and $\widetilde{\Omega}_{k_1,2m-1} = v$, the Hamiltonian (1) can be recast into the following two-leg-coupled SSH model:

$$
\begin{aligned}
\hat{H} = {} & \sum_{j=1}^N (v\hat{a}_{j,0}^\dagger \hat{b}_{j,0} + w\hat{a}_{j,1}^\dagger \hat{b}_{j,1} + t_1 \hat{a}_{j,0}^\dagger \hat{a}_{j,1} + t_2 \hat{b}_{j,0}^\dagger \hat{b}_{j,1}) \\
& + \sum_{j=1}^{N-1} (w\hat{a}_{j+1,0}^\dagger \hat{b}_{j,0} + v\hat{a}_{j+1,1}^\dagger \hat{b}_{j,1}) + \text{H.c.}, \quad (2)
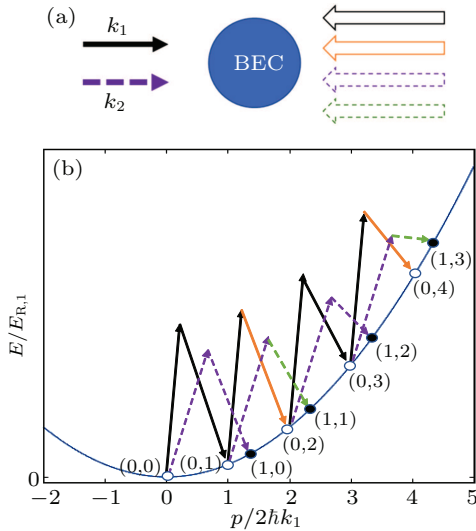\end{aligned}
$$

Fig. 1. (a) Sketch of the proposed experimental setup. The counterpropagating lasers form a set of Raman structures inducing transitions between different momentum states. The solid and dotted lines represent the laser fields with wave numbers k_1 and k_2, respectively. Different colors represent different Rabi frequencies. (b) Free-particle dispersion relation and recoil energy $E_{\text{R},1} = \hbar^2 k^2/2M$. The open and filled circles represent the momentum states in legs $n = 0$ and $n = 1$, respectively. The intraleg and interleg transitions are controlled by lasers with wave numbers k_1 and k_2, respectively.

where the field operator $\hat{\alpha}_{j,n}$ ($\hat{\alpha}_{j,n}^\dagger$) annihilate (create) a particle at sublattice α ($= a, b$) of the n-th leg and j-th unit cell. The intraleg (interleg) hopping strengths are denoted by v and w (t_1 and t_2). The Hamiltonian (2) describes two-leg-coupled SSH chains with staggered interleg hoppings and opposite dimerizations. The system respects a glide reflection symmetry and a mirror symmetry for $t_1 = t_2$.[47,48] We set $t_1 = 1$ as the unit of energy hereafter.
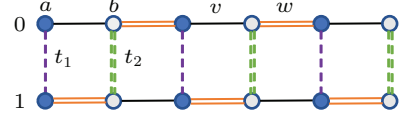

Fig. 2. Sketch of the tight-binding model. The model consists of two legs $n = 0$ and 1, each of which constitutes a SSH type chain. t_1 and t_2 are the staggered interleg hoppings. v and w are the intracell and intercell hoppings within one leg.

3. Energy spectrum and winding number

To catch some insight into the topological property of the system, we first plot the energy spectrum of Hamiltonian (2) with open boundary condition. As shown in Fig. 3, two zero-energy states appear in the gap for $(w+v)^2 > t_1 t_2$ and $w < v$. As w increases, these two zero-modes first merge into the bulk band at $w = v$, and then reappear for $w > v$. The zero-mode pairs for $w < v$ and $w > v$ are both deep inside the band gaps [see the top panels of Figs. 3(b) and 3(c)], whereas their population distributions behave distinctly. This is illustrated in the bottom panels of Figs. 3(b) and 3(c). It can be seen that for $w = 0.6$, the population distributions are mainly localized at the four fock basis $\hat{a}_{1,1}^\dagger |0\rangle$, $\hat{a}_{20,0}^\dagger |0\rangle$, $\hat{b}_{1,0}^\dagger |0\rangle$ and $\hat{b}_{20,1}^\dagger |0\rangle$, whereas for $w = 1.6$, the zero modes populate $\hat{b}_{1,1}^\dagger |0\rangle$, $\hat{b}_{20,0}^\dagger |0\rangle$, $\hat{a}_{1,0}^\dagger |0\rangle$ and $\hat{a}_{20,1}^\dagger |0\rangle$ instead. The physics behind this phenomenon will be detailed in Section 4.

The bulk property can be conveniently captured by considering the periodic boundary condition. To this end, we apply a Fourier transformation, $\hat{\alpha}_{j,n} = 1/\sqrt{N/2} \sum_k e^{ikj} \hat{\alpha}_{k,n}$ to write the Hamiltonian into the Bloch space as

$$
\hat{H}_k = \hat{\psi}_k^\dagger \hat{H}(k) \hat{\psi}_k, \quad (3)
$$

where $\hat{\psi}_k = (\hat{a}_{k,0}, \hat{b}_{k,0}, \hat{a}_{k,1}, \hat{b}_{k,1},)^{\text{T}}$ and

$$
\begin{aligned}
H(k) &= \begin{pmatrix}
0 & 0 & t_1 & w + v e^{-ik} \\
0 & 0 & v + w e^{ik} & t_2 \\
t_1 & v + w e^{-ik} & 0 & 0 \\
w + v e^{ik} & t_2 & 0 & 0
\end{pmatrix} \\
&= \begin{pmatrix} 0 & h^\dagger \\ h & 0 \end{pmatrix}. \quad (4)
\end{aligned}
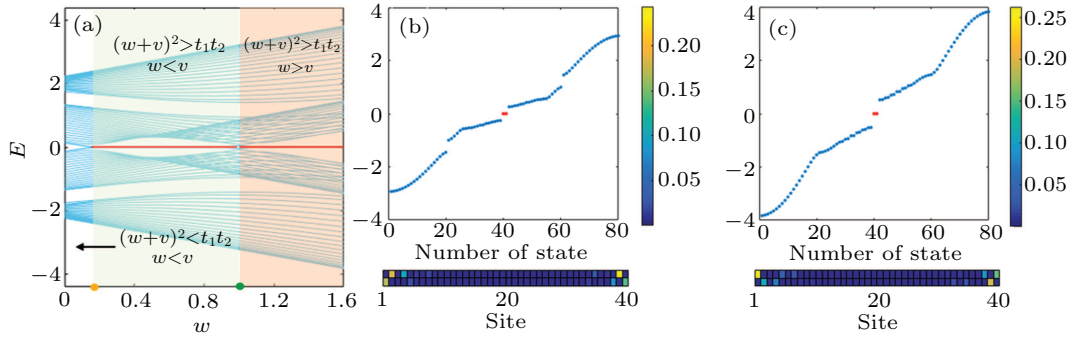$$

Here T is a transport operator.

Fig. 3. (a) Energy spectrum of the two-leg-coupled SSH model under open boundary condition with 20 unit cells, the other parameters are $v = 1$ and $t_2 = 1.4$. The red line denotes the zero-energy mode. The yellow and green dots are the points where the band gap closes ($w = \sqrt{t_1 t_2} - v \approx 0.18$ and $w = v = 1$). The top panels of (b) and (c) are the eigenenergy with $w = 0.6$ and $w = 1.6$, respectively. The bottom panels of (b) and (c) depict the density population of the edge states with $w = 0.6$ and $w = 1.6$, respectively.

Diagonalizing Hamiltonian (4), we obtain the eigenenergy

$$E(k) = \pm \sqrt{M/2 \pm \sqrt{M^2/4 - D}}, \qquad (5)$$

where $M = t_1^2 + t_2^2 + 2(v^2 + w^2 + 2vw \cos k)$ and $D = t_1^2 t_2^2 + (v^2 + w^2 + 2vw \cos k)^2 - 2t_1 t_2 [2vw + (v^2 + w^2) \cos k]$. Figures 4(a)–4(d) plot the band structure $E(k)$ with $t_2 = 1.4$, $v = 0.8$ and various w. It is to be seen that the system host four different bands, out of which the two lowest (highest) ones have no intersections at the edge of the first Brillouin zone due to the breaking of glide reflection symmetry. As shown in Fig. 4(a), the band gap keeps open for weak w. However, as w is increased from weak to strong, the system successively exhibits gap closing [Fig. 4(b)], gap reopening [Fig. 4(c)], and gap reclosing [Fig. 4(d)], signaling that the topological phase transitions may happen twice. The fate of
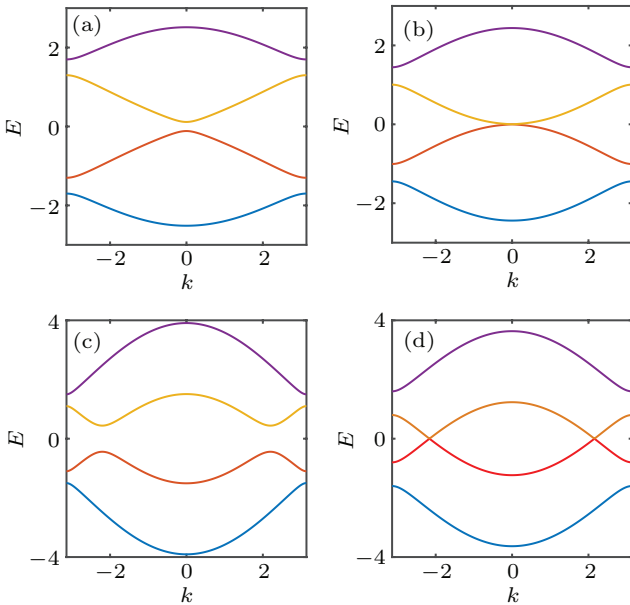
the gap-closing points can be unveiled by inspecting the equation $E(k) = 0$, from which we find that the band gap closes at a single point $k_c = 0$ [two points $k_c = \pm \arccos(t_1 t_2 / 2v^2 - 1)$] when $(w + v)^2 = t_1 t_2$ [$(w + v)^2 > t_1 t_2$ and $v = w$].
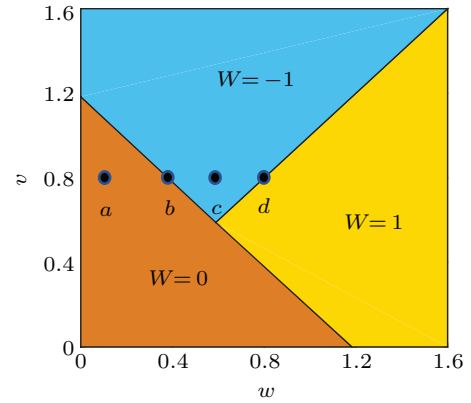

Fig. 5. Phase diagram on the v–w plane with $t_1 t_2 = 1.4$. The points a–d correspond to band structures in Figs. 4(a)–4(d).

It is straight forward to show that the Hamiltonian (4) exhibits the following sublattice symmetry:

$$\hat{\Gamma} \hat{H}(k) \hat{\Gamma}^{-1} = -\hat{H}(k), \qquad (6)$$

where $\hat{\Gamma} = \hat{\tau}_3 \otimes \hat{I}$ is the sublattice operator. The sublattice symmetry presented in Eq. (6), together with the time-reversal [$\hat{H}^*(k) = \hat{H}(-k)$] and particle–hole [$\hat{\Gamma} \hat{H}^*(k) \hat{\Gamma}^{-1} = -\hat{H}(-k)$] symmetries, guarantees that the system belongs to the BDI symmetry class according to "tenfold way".[6] Hence, the topological invariant is the winding number[1]

$$W = \int \frac{\mathrm{d}k}{2\pi \mathrm{i}} \mathrm{Tr} \left[h^{-1} d_k h \right], \qquad (7)$$

with which we numerically map out the full phase diagram in Fig. 5. It can be seen that, depending on different parameters, the winding number can take 1, 0 and -1 representing different topological phases. This can also be understood analytically by expressing Eq. (7) as

$$W = \int \frac{\mathrm{d}k}{2\pi \mathrm{i}} d_k \ln \{\mathrm{Det}[h(k)]\} = \arg \{\mathrm{Det}[h(k)]\} / 2\pi \big|_{-\pi}^{\pi}, \quad (8)$$

Fig. 4. Plots of the energy band under periodic boundary condition with $t_2 = 1.4$, $v = 0.8$ and (a) $w = 0.1$, (b) $w = 0.4$, (c) $w = 0.6$ and (d) $w = 0.8$. (a) and (c), both with a nonzero band gap, correspond to topological trivial and non-trivial cases, respectively; (b) and (d) show a gapless band structure, signaling the appearance of topological phase boundary.

where

$$\mathrm{Det}|h(k)| = t_1 t_2 - 2vw - (v^2 + w^2)\cos k - \mathrm{i}(w^2 - v^2)\sin k. \quad (9)$$

The determinant (9) defines a map: $S^1 \to C$. Because of $h(-\pi) = h(\pi)$, the map forms a closed smooth curve on the complex plane

$$
\begin{aligned}
x &= t_1 t_2 - 2vw - (v^2 + w^2)\cos k, \\
y &= -(w^2 - v^2)\sin k,
\end{aligned} \quad (10)
$$

which gives rise to an elliptic equation defined by

$$\frac{[x - (t_1 t_2 - 2vw)]^2}{(v^2 + w^2)^2} + \frac{y^2}{(w^2 - v^2)^2} = 1. \quad (11)$$

The semi-major axis of the ellipse is $a = (w^2 + v^2)$ and the center is $(t_1 t_2 - 2vw, 0)$. While for $(w+v)^2 < t_1 t_2$, the ellipse does not go around the origin leading to zero winding number, the ellipse goes around the origin if $(w+v)^2 > t_1 t_2$, which produces non-zero winding number ± 1. The sign of the non-zero winding number is controlled by the direction of the curve governed by Eq. (10). That is, as k increases, $\mathrm{Det}|h(k)|$ goes clockwise (anticlockwise) around the origin for $v > w$ ($v < w$), yielding $W = 1$ ($W = -1$).

4. Edge state solutions

We now give an analytical expression of the edge states, which has been numerically depicted in Fig. 3, to unambiguously demonstrate their type-II character. The eigenstates of Hamiltonian (2) assume the general form

$$
\begin{aligned}
\Psi = \sum_j (&\psi_{(a,0),j}\hat{a}^\dagger_{j,0} + \psi_{(b,0),j}\hat{b}^\dagger_{j,0} \\
&+ \psi_{(a,1),j}\hat{a}^\dagger_{j,1} + \psi_{(b,1),j}\hat{b}^\dagger_{j,1})|0\rangle.
\end{aligned} \quad (12)
$$

The edge states are zero mode satisfying $\hat{H}\Psi = 0$, which yields

$$
\begin{aligned}
w\psi_{(b,1),j} + v\psi_{(b,1),j-1} + t_1\psi_{(a,0),j} &= 0, \quad (13) \\
w\psi_{(a,0),j+1} + v\psi_{(a,0),j} + t_2\psi_{(b,1),j} &= 0, \quad (14) \\
v\psi_{(b,0),j} + w\psi_{(b,0),j-1} + t_1\psi_{(a,1),j} &= 0, \quad (15) \\
v\psi_{(a,1),j+1} + w\psi_{(a,1),j} + t_2\psi_{(b,0),j} &= 0. \quad (16)
\end{aligned}
$$

The form of the sublattice operator $\hat{\Gamma}$ motivates us to divide the whole Hilbert space into two subspaces I and II, which are characterized by the basis sets $\mathrm{I} = \{\hat{a}_{j,0}|0\rangle, \hat{b}_{j,1}|0\rangle\}$ and $\mathrm{II} = \{\hat{a}_{j,1}|0\rangle, \hat{b}_{j,0}|0\rangle\}$, respectively. Notice that subspace I and subspace II are completely decoupled and host opposite recursive structures, i.e., the roles of w and v interchange in Eqs. (13) and (15). This implies that the wavefunctions belonging to the two subspaces will exhibit opposite asymptotic behaviors. According to the theory of difference equations, we have

$$
\psi_{(a,0),j} = \begin{cases} A_1\alpha_1^j - A_2\beta_1^j, & t_1 t_2 > 4vw, \\ (A_1 + A_2 j)\left(\frac{v}{w}\right)^j, & t_1 t_2 = 4vw, \\ \mathrm{e}^{j\ln\frac{v}{w}}(A_1\cos j\phi + A_2\sin j\phi), & t_1 t_2 < 4vw, \end{cases} \quad (17)
$$

$$
\psi_{(b,1),j} = \begin{cases} B_1\alpha_1^j - B_2\beta_1^j, & t_1 t_2 > 4vw, \\ (B_1 + B_2 j)\left(\frac{v}{w}\right)^j, & t_1 t_2 = 4vw, \\ \mathrm{e}^{j\ln\frac{v}{w}}(B_1\cos j\phi + B_2\sin j\phi), & t_1 t_2 < 4vw, \end{cases} \quad (18)
$$

$$
\psi_{(b,0),j} = \begin{cases} C_1\alpha_2^j - C_2\beta_2^j, & t_1 t_2 > 4vw, \\ (C_1 + C_2 j)\left(\frac{w}{v}\right)^j, & t_1 t_2 = 4vw, \\ \mathrm{e}^{j\ln\frac{w}{v}}(C_1\cos j\theta + C_2\sin j\theta), & t_1 t_2 < 4vw, \end{cases} \quad (19)
$$

$$
\psi_{(a,1),j} = \begin{cases} D_1\alpha_2^j - D_1\beta_2^j, & t_1 t_2 > 4vw, \\ (D_1 + D_2 j)\left(\frac{w}{v}\right)^j, & t_1 t_2 = 4vw, \\ \mathrm{e}^{j\ln\frac{w}{v}}(D_1\cos j\theta + D_2\sin j\theta), & t_1 t_2 < 4vw, \end{cases} \quad (20)
$$

where $\alpha_1 = [(t_1 t_2 - 2vw) + \sqrt{t_1^2 t_2^2 - 4vw t_1 t_2}]/2w^2$, $\beta_1 = [(t_1 t_2 - 2vw) - \sqrt{t_1^2 t_2^2 - 4vw t_1 t_2}]/2w^2$. α_2 (β_2) assumes the same form of α_1 (β_1) but with $v \leftrightarrow w$. The semi-infinite boundary condition fixes the left edge as $\psi_{(a,0),0} = \psi_{(a,1),0} = \psi_{(b,0),0} = \psi_{(b,1),0} = 0$. This imposes a constraint on the coefficients such that for $t_1 t_2 > 4vw$, $Y_1 = -Y_2$ and otherwise $Y_1 = 0$ ($Y = A, B, C, D$). Therefore, from Eqs. (13)–(16), we have

$$
\begin{cases} w\psi_{(b,1),1} + t_1\psi_{(a,0),1} = 0, \\ v\psi_{(b,0),1} + t_1\psi_{(a,1),1} = 0. \end{cases} \quad (21)
$$

This means (i) $\psi_{(b,1),1} = \psi_{(a,0),1} = \psi_{(b,0),1} = \psi_{(a,1),1} = 0$ or (ii) $\psi_{(a,0),1}/\psi_{(b,1),1} = -w/t_1$ and $\psi_{(a,1),1}/\psi_{(b,0),1} = -v/t_1$. According to the above analysis, we obtain

$$
\psi_{(a,0),j} = \begin{cases} A(\alpha_1^j - \beta_1^j), & t_1 t_2 > 4vw, \\ A j\left(\frac{v}{w}\right)^j, & t_1 t_2 = 4vw, \\ A\,\mathrm{e}^{j\ln\frac{v}{w}}\sin j\phi, & t_1 t_2 < 4vw, \end{cases} \quad (22)
$$

$$
\psi_{(b,1),j} = \begin{cases} -A\left(\frac{t_1}{w}\right)(\alpha_1^j - \beta_1^j), & t_1 t_2 > 4vw, \\ -A\left(\frac{t_1}{w}\right) j\left(\frac{v}{w}\right)^j, & yt_1 t_2 = 4vw, \\ -A\left(\frac{t_1}{w}\right)\mathrm{e}^{j\ln\frac{v}{w}}\sin j\phi, & t_1 t_2 < 4vw, \end{cases} \quad (23)
$$

$$
\psi_{(b,0),j} = \begin{cases} B(\alpha_2^j - \beta_2^j), & t_1 t_2 > 4vw, \\ B j\left(\frac{w}{v}\right)^j, & t_1 t_2 = 4vw, \\ B\,\mathrm{e}^{j\ln\frac{w}{v}}\sin j\theta, & t_1 t_2 < 4vw, \end{cases} \quad (24)
$$

$$
\psi_{(a,1),j} = \begin{cases} -B\left(\frac{v}{t_1}\right)(\alpha_2^j - \beta_2^j), & t_1 t_2 > 4vw, \\ -B\left(\frac{v}{t_1}\right) j\left(\frac{w}{v}\right)^j, & t_1 t_2 = 4vw, \\ -B\left(\frac{v}{t_1}\right)\mathrm{e}^{j\ln\frac{w}{v}}\sin j\theta, & t_1 t_2 < 4vw, \end{cases} \quad (25)
$$

which gives $\psi_{(b,1),j} = -(t_1/w)\psi_{(a,0),j}$ and $\psi_{(a,1),j} = -(v/t_1)\psi_{(b,0),j}$. It can be seen from Eqs. (22) and (24) that, for $v > w$ ($v < w$), $\psi_{(b,0),j}$ ($\psi_{(a,0),j}$) decreases to zero and $\psi_{(a,0),j}$ ($\psi_{(b,0),j}$) increases to infinity as j increases. As a result, the edge states can not occupy both subspace I and subspace II at a single end. Moreover, if the edge states occupy subspace I at the left end, they will occupy subspace II at the right end, and vice versa.

5. Possible experimental observation

We now propose a dynamical scheme to experimentally detect the topological winding number and edge states.

In an experiment, the winding number can be conveniently captured by the chiral displacement (CD),[49,50] $C(t) = \langle \Gamma_{\text{tol}} X \rangle$, where X is the position operator of the unit cell and $\Gamma_{\text{tol}} = \bigoplus^N \Gamma$ is the total sublattice operator. Since $C(t)$ is sensitive to the choice of the initial state, to be concrete, let us denote $C_{\mu,n}^j(t)$ as the CD obtained from the state initialized at the sublattice (μ, n) ($\mu = a, b$ and $n = 0, 1$) of unit cell j. We thus introduce an extended CD defined at the unit cell j as the addition of the two independent trajectories: $C^j(t) = C_{a,0}^j(t) + C_{b,1}^j(t)$. It is found that the long-time-averaged CD, namely, $\bar{C} = \lim_{T \to \infty}(1/T)\int_0^T C^j(t)\,dt$, gives nothing but the topological winding number. Figure 6 shows the numerical simulations of $\bar{C}$ with $N = 10$ and $T = 5$ ms. The time evolutions of $C^j(t)$ for two representative parameter regimes are shown in the left and right insets. It is clear that the long-time-averaged CD can indeed provide correct predictions about the winding number and the corresponding topological phase transitions. In our model, we begin with all lasers turned off and prepare the initial states at the central unit cell. Explicitly, the two initial states are $\psi_1 = (0, \ldots, 0, \mathbf{1}, \mathbf{0}, \mathbf{0}, \mathbf{0}, 0, \ldots, 0)$

and $\psi_2 = (0, \ldots, 0, \mathbf{0}, \mathbf{0}, \mathbf{0}, \mathbf{1}, 0, \ldots, 0)$. The corresponding mean chiral displacements are $C_{a,0}^0(t)$ and $C_{b,1}^0(t)$. Then, we suddenly turn on the Raman couplings. As the evolution of the system is determined by the Hamiltonian (2), we can evaluate $C_{a,0}^0(t)$ and $C_{b,1}^0(t)$ by a series of absorption images of the atomic population distribution.
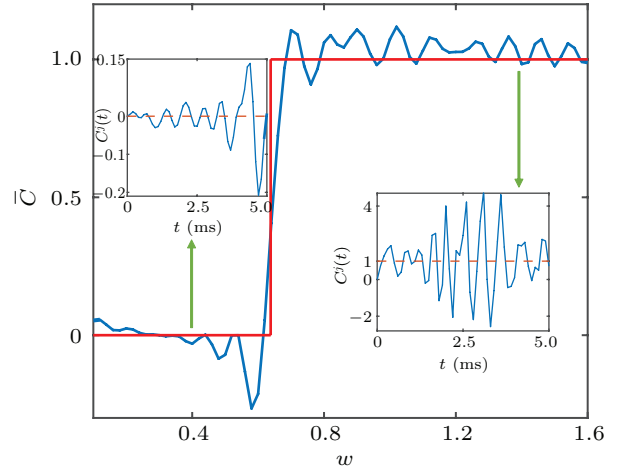

Fig. 6. The time-averaged chiral displacement as a function of w. The red line is the theoretical prediction of the winding number. The blue line is the numerical simulation with $N = 10$. The insets show the chiral displacement as a function of time. The other parameters are the same as those in Fig. 3.
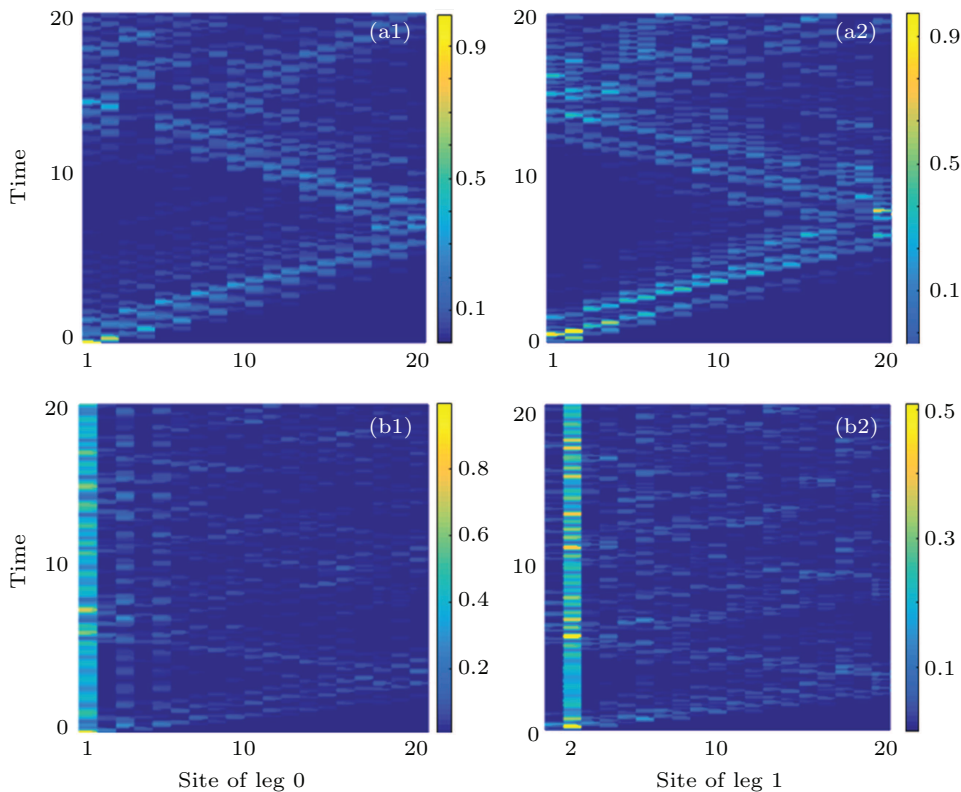
Fig. 7. Population dynamics of the single-particle state initialized at the sublattice $(a, 0)$ of the first unit cell with $v = 0.6$, $t_2 = 1.4$ and $N = 10$. (a1) [(a2)] plots the atomic distribution on leg 0 (leg 1) with $w = 0.2$. (b1) and (b2) are the same as (a1) and (a2) but with $w = 1.2$.

The edge state can be detected by monitoring the atomic distribution on different momentum states. In experiment, we can suddenly turn off all laser beams, such that atoms evolve to different momentum states. Then we measure the absorption image and count the number of atoms in the different momentum states. For example, for a BEC initially prepared at

the zero momentum state, the Raman couplings can be conveniently designed to produce a momentum lattice in which the initial state populates the sublattice $(a, 0)$ of the first unit cell. Therefore, the localization of the BEC on its initial state is a clear signature of the presence of edge state. As shown in Fig. 7, we numerically calculate the dynamics of the atomic distribution for a BEC initialized at the zero momentum state for different coupling parameters. It is seen that, for $(w + v)^2 > t_1 t_2$ [Figs. 7(b1) and 7(b2)], the BEC is localized at the sublattices $(a, 0)$ and $(b, 1)$ of the first unit cell, whereas it extends to the whole lattice sites for $(w + v)^2 < t_1 t_2$ [Figs. 7(a1) and 7(a2)].

6. Conclusion

In summary, we have proposed a feasible experimental scheme to study the topological properties of a two-leg-coupled SSH model with staggered interleg hopping. It is found that this model supports two nontrivial topological phases and a trivial phase. By solving the eigenequations, we have predicted the presence of a type-II edge state. This can be regarded as an analog of type-II corner state in two dimension. Based on the relationship between edge state and topological invariant, we have built the bulk–boundary correspondence in our system. Moreover, possible experimental observation of the edge states and bulk topological invariants have been addressed.

Appendix A

The laser beams that generate the coupled SSH chain in momentum space take the following form:

$$\boldsymbol{E}_1^+ (x, t) = \boldsymbol{E}_1^+ \cos\left(k_1^+ \hat{x} - \omega_1^+ t + \phi_1^+\right), \tag{A1}$$

$$\boldsymbol{E}_1^- (x, t) = \sum_i \boldsymbol{E}_{1i}^- \cos\left(k_{1i}^- \hat{x} - \omega_{1i}^- t + \phi_{1i}^-\right), \tag{A2}$$

$$\boldsymbol{E}_2^+ (x, t) = \boldsymbol{E}_2^+ \cos\left(k_2^+ \hat{x} - \omega_2^+ t + \phi_2^+\right), \tag{A3}$$

$$\boldsymbol{E}_2^- (x, t) = \sum_i \boldsymbol{E}_{2i}^- \cos\left(k_{2i}^- \hat{x} - \omega_{2i}^- t + \phi_{2i}^-\right), \tag{A4}$$

$$\boldsymbol{E} = \boldsymbol{E}_1 + \boldsymbol{E}_2. \tag{A5}$$

The Hamiltonian of the free atoms reads

$$\begin{aligned}
\hat{H}_{\mathrm{A}} &= \frac{\hat{P}^2}{2m} + \hbar \omega_e |e\rangle\langle e| + \hbar \omega_g |g\rangle\langle g| \\
&= \frac{\hat{P}^2}{2M} + \hbar \omega_{eg} |e\rangle\langle e|,
\end{aligned} \tag{A6}$$

where $\omega_{eg} = \omega_e - \omega_g$ and we have taken the ground state to be zero energy. The atom–field interaction under dipole approximations is described by

$$\hat{H}_{\mathrm{int}} = -\boldsymbol{d} \cdot \boldsymbol{E}, \tag{A7}$$

where $\boldsymbol{d}$ is the atomic dipole operator. Applying the rotating-wave approximation and transforming into a rotating frame, the total Hamiltonian becomes

$$\hat{H} = \hat{H}_{\mathrm{A}} + \hat{H}_{\mathrm{int}} = \frac{\hat{P}^2}{2m} + \hbar \Delta |e\rangle\langle e|$$

$$\begin{aligned}
&+ \frac{\hbar}{2}\left[\Omega_1^+ \left(\sigma^+ \mathrm{e}^{\mathrm{i}k_1^+ \hat{x}} \mathrm{e}^{\mathrm{i}\phi_1^+} + \sigma^- \mathrm{e}^{-\mathrm{i}k_1^+ \hat{x}} \mathrm{e}^{-\mathrm{i}\phi_1^+}\right) \right. \\
&+ \sum_i \Omega_{1i}^- \left(\sigma^+ \mathrm{e}^{\mathrm{i}k_{1i}^- \hat{x}} \mathrm{e}^{\mathrm{i}[(\omega_1^+ - \omega_{1i}^-)t + \phi_{1i}^-]}\right. \\
&+ \left.\sigma^- \mathrm{e}^{-\mathrm{i}k_{1i}^- \hat{x}} \mathrm{e}^{-\mathrm{i}[(\omega_1^+ - \omega_{1i}^-)t + \phi_{1i}^-]}\right) \\
&+ \Omega_2^+ \left(\sigma^+ \mathrm{e}^{\mathrm{i}k_2^+ \hat{x}} \mathrm{e}^{\mathrm{i}[(\omega_1^+ - \omega_2^+)t + \phi_2^+]}\right. \\
&+ \left.\sigma^- \mathrm{e}^{-\mathrm{i}k_2^+ \hat{x}} \mathrm{e}^{-\mathrm{i}[(\omega_1^+ - \omega_2^+)t + \phi_2^+]}\right) \\
&+ \sum_i \Omega_{2i}^- \left(\sigma^+ \mathrm{e}^{\mathrm{i}k_{2i}^- \hat{x}} \mathrm{e}^{\mathrm{i}[(\omega_1^+ - \omega_{2i}^-)t + \phi_{2i}^-]}\right. \\
&+ \left.\left.\sigma^- \mathrm{e}^{-\mathrm{i}k_{2i}^- \hat{x}} \mathrm{e}^{-\mathrm{i}[(\omega_1^+ - \omega_{2i}^-)t + \phi_{2i}^-]}\right)\right],
\end{aligned} \tag{A8}$$

where $\Delta \equiv \omega_{eg} - \omega_1^+$ is the single photon detuning. The Schrödinger equation under the Hamiltonian (A8) is

$$\begin{aligned}
&\mathrm{i}\hbar \partial_t \left|\varphi_g(t)\right\rangle \\
&= \frac{\hat{P}^2}{2m} \left|\varphi_g(t)\right\rangle + \frac{\hbar}{2}\left[\Omega_1^+ \mathrm{e}^{-\mathrm{i}k_1^+ \hat{x}} \mathrm{e}^{-\mathrm{i}\phi_1^+}\right. \\
&+ \sum_i \Omega_{1i}^- \mathrm{e}^{-\mathrm{i}k_{1i}^- \hat{x}} \mathrm{e}^{-\mathrm{i}[(\omega_1^+ - \omega_{1i}^-)t + \phi_{1i}^-]} \\
&+ \Omega_2^+ \mathrm{e}^{-\mathrm{i}k_2^+ \hat{x}} \mathrm{e}^{-\mathrm{i}[(\omega_1^+ - \omega_2^+)t + \phi_2^+]} \\
&+ \left.\sum_i \Omega_{2i}^- \mathrm{e}^{-\mathrm{i}k_{2i}^- \hat{x}} \mathrm{e}^{-\mathrm{i}[(\omega_1^+ - \omega_{2i}^-)t + \phi_{2i}^-]}\right] \left|\varphi_e(t)\right\rangle,
\end{aligned} \tag{A9}$$

$$\begin{aligned}
&\mathrm{i}\hbar \partial_t \left|\varphi_e(t)\right\rangle \\
&= \frac{\hat{P}^2}{2m} \left|\varphi_e(t)\right\rangle + \hbar \Delta \left|\varphi_e(t)\right\rangle \\
&+ \frac{\hbar}{2}\left[\Omega_1^+ \mathrm{e}^{\mathrm{i}k_1^+ \hat{x}} \mathrm{e}^{\mathrm{i}\phi_1^+}\right. \\
&+ \sum_i \Omega_{1i}^- \mathrm{e}^{\mathrm{i}k_{1i}^- \hat{x}} \mathrm{e}^{\mathrm{i}[(\omega_1^+ - \omega_{1i}^-)t + \phi_{1i}^-]} \\
&+ \Omega_2^+ \mathrm{e}^{\mathrm{i}k_2^+ \hat{x}} \mathrm{e}^{\mathrm{i}[(\omega_1^+ - \omega_2^+)t + \phi_2^+]} \\
&+ \left.\sum_i \Omega_{2i}^- \mathrm{e}^{\mathrm{i}k_{2i}^- \hat{x}} \mathrm{e}^{\mathrm{i}[(\omega_1^+ - \omega_{2i}^-)t + \phi_{2i}^-]}\right] \left|\varphi_g(t)\right\rangle.
\end{aligned} \tag{A10}$$

Tuning the single photon detuning Δ such that it is much larger than the characteristic energy of other degrees of freedom, we can safely eliminate the excited state $|e\rangle$ by setting $\mathrm{i}\hbar \partial_t |\varphi_e(t)\rangle = 0$, yielding

$$\begin{aligned}
&\mathrm{i}\hbar \partial_t \left|\varphi_g(t)\right\rangle \\
&= \frac{\hat{P}^2}{2m} \left|\varphi_g(t)\right\rangle - \frac{\hbar}{4\Delta}\left[\Omega_1^+ \mathrm{e}^{-\mathrm{i}(k_1^+ \hat{x} - \phi_1^+)}\right. \\
&+ \sum_i \Omega_{1i}^- \mathrm{e}^{-\mathrm{i}k_{1i}^- \hat{x}} \mathrm{e}^{-\mathrm{i}[(\omega_1^+ - \omega_{1i}^-)t + \phi_{1i}^-]} \\
&+ \Omega_2^+ \mathrm{e}^{-\mathrm{i}k_2^+ \hat{x}} \mathrm{e}^{-\mathrm{i}[(\omega_1^+ - \omega_2^+)t + \phi_2^+]} \\
&+ \left.\sum_i \Omega_{2i}^- \mathrm{e}^{-\mathrm{i}k_{2i}^- \hat{x}} \mathrm{e}^{-\mathrm{i}[(\omega_1^+ - \omega_{2i}^-)t + \phi_{2i}^-]}\right]\left[\Omega_1^+ \mathrm{e}^{\mathrm{i}(k_1^+ \hat{x} + \phi_1^+)}\right. \\
&+ \sum_i \Omega_{1i}^- \mathrm{e}^{\mathrm{i}[k_{1i}^- \hat{x} + (\omega_1^+ - \omega_{1i}^-)t + \phi_{1i}^-]} \\
&+ \Omega_2^+ \mathrm{e}^{\mathrm{i}k_2^+ \hat{x}} \mathrm{e}^{\mathrm{i}[(\omega_1^+ - \omega_2^+)t + \phi_2^+]} \\
&+ \left.\sum_i \Omega_{2j}^- \mathrm{e}^{\mathrm{i}k_{2i}^- \hat{x}} \mathrm{e}^{\mathrm{i}[(\omega_1^+ - \omega_{2i}^-)t + \phi_{2i}^-]}\right] \left|\varphi_g(t)\right\rangle.
\end{aligned} \tag{A12}$$

The effective Hamiltonian can be readily read out from Eq. (A8) as

$$\hat{H}_{eff} = \frac{\hat{P}^2}{2m} - \left[\frac{\hbar\left(\Omega_1^+\right)^2}{4\Delta} + \sum_i \frac{\hbar\left(\Omega_{1i}^-\right)^2}{4\Delta} + \frac{\hbar\left(\Omega_2^+\right)^2}{4\Delta} + \sum_i \frac{\hbar\left(\Omega_{2i}^-\right)^2}{4\Delta} \right]$$

$$- \hbar \sum_i \left(\frac{\Omega_{1i}^-\Omega_1^+}{4\Delta} e^{i2k_1\hat{x}} e^{i[-(\omega_1^+ - \omega_{1i}^-)t + (\phi_1^+ - \phi_{1i}^-)]} + \frac{\Omega_{2i}^-\Omega_1^+}{4\Delta} e^{iq\hat{x}} e^{i[-(\omega_1^+ - \omega_{2i}^-)t + (\phi_1^+ - \phi_{2i}^-)]} \right)$$

$$- \hbar \sum_i \left(\frac{\Omega_{1i}^-\Omega_2^+}{4\Delta} e^{iq\hat{x}} e^{i[-(\omega_2^+ - \omega_{1i}^-)t + (\phi_2^+ - \phi_{1i}^-)]} + \frac{\Omega_{2i}^-\Omega_2^+}{4\Delta} e^{i2k_2\hat{x}} e^{i[-(\omega_2^+ - \omega_{2i}^-)t + (\phi_2^+ - \phi_{2i}^-)]} \right)$$

$$- \hbar \left(\frac{\Omega_1^+\Omega_2^+}{4\Delta} e^{ip\hat{x}} e^{i[-(\omega_1^+ - \omega_2^+)t + (\phi_1^+ - \phi_2^+)]} + \sum_{i,i'} \frac{\Omega_{1i}^-\Omega_{2i'}^-}{4\Delta} e^{-ip\hat{x}} e^{i[(\omega_{2i'}^- - \omega_{1i}^-)t + (\phi_{1i}^- - \phi_{2i'}^-)]} \right)$$

$$- \hbar \sum_{i \neq i'} \frac{\Omega_{1i}^-\Omega_{1i'}^-}{4\Delta} e^{i[(\omega_{1i}^- - \omega_{1i'}^-t) + (\phi_{1i'}^- - \phi_i^-)]} - \hbar \sum_{i \neq i'} \frac{\Omega_{2i}^-\Omega_{2i'}^-}{4\Delta} e^{i[(\omega_{2i}^- - \omega_{2i'}^-)t + (\phi_{2i'}^- - \phi_{2i}^-)]}, \tag{A13}$$

where $k_1 = k_1^+ = -k_{1j}^-$, $k_2 = k_2^+ = -k_{2j}^-$, $p = k_1 - k_2$, and $q = k_1 + k_2$.

We now define a discrete basis of relevant plan-wave momentum states $|m,n,r,s\rangle$ (with m, n, r and s being integers), having momenta $p_{m,n,r,s} = \hbar(2mk_1 + 2nk_2 + rp + sq)$. Choosing k_1/k_2 to be irrational, we can write the complete basis in momentum space as

$$I = \sum_{m,n,r,s} |m,n,r,s\rangle \langle m,n,r,s|. \tag{A14}$$

Under the basis represented by Eq. (A14), the diagonal and off-diagonal terms of Hamiltonian (A13) are respectively given as

$$\hat{H}_{\text{dia}}(p) = \sum_{m,n,x,y} \frac{(2m\hbar k_1 + 2n\hbar k_2 + xp + yq)^2}{2m}$$
$$\times |m,n,x,y\rangle \langle m,n,x,y|, \tag{A15}$$

and

$$\hat{H}_{\text{off}}(p) = \hbar \left[\sum_{m,n,x,y} \sum_i \widetilde{\Omega}_{1i} e^{i\widetilde{\phi}_{1i}} e^{-i(\omega_1^+ - \omega_{1i}^-)t} |m+1\rangle\langle m| + \sum_{m,n,x,y} \sum_i \widetilde{\Omega}_{2i} e^{i\widetilde{\phi}_{2i}} e^{-i(\omega_2^+ - \omega_{2i}^-)t} |n+1\rangle\langle n| \right.$$

$$+ \sum_{m,n,x,y} \sum_i \widetilde{\Omega}_i^2 e^{i\widetilde{\phi}_i^2} e^{-i(\omega_2^+ - \omega_{1i}^-)t} |y+1\rangle\langle y| + \sum_{m,n,x,y} \sum_i \widetilde{\Omega}_i^1 e^{i\widetilde{\phi}_i^1} e^{-i(\omega_1^+ - \omega_{2i}^-)t} |y+1\rangle\langle y|$$

$$\left. + \sum_{m,n,x,y} \widetilde{\Omega}_{12} e^{i(\phi_1^+ - \phi_2^+)} e^{-i(\omega_1^+ - \omega_2^+)t} |x+1\rangle\langle x| + \sum_{m,n,x,y,i,i'} \frac{\Omega_{1i}^-\Omega_{2i'}^-}{4\Delta} e^{i[(\omega_{2i'}^- - \omega_{1i}^-)t + \widetilde{\phi}_{i,i'}]} |x+1\rangle\langle x| + \text{H.c} \right]. \tag{A6}$$

where $\widetilde{\Omega}_{li} = \frac{\Omega_{li}^-\Omega_l^+}{4\Delta}$, $\widetilde{\phi}_{li} = \phi_l^+ - \phi_{li}^-$, $\widetilde{\Omega}_i^l = \frac{\Omega_{li}^-\Omega_l^+}{4\Delta}$, $\widetilde{\phi}_i^l = \phi_l^+ - \phi_{li}^-$, $\widetilde{\Omega}_{12} = \frac{\Omega_1^+\Omega_2^+}{4\Delta}$. Note that in writing the momentum basis in Hamiltonians (A15) and (A6), we have ignored the irrelevant quantum numbers which keep invariant. Moving into an interaction picture characterized by the unitary transition $U_P = \exp\left(\frac{-i}{\hbar}\hat{H}_0(p)t\right)$, the total Hamiltonian can be written as

$$\hat{H}_I(p) = i\hbar \frac{dU_P^\dagger}{dt}U_P + U_P^\dagger \hat{H}(p)U_P = i\hbar \frac{dU_P^\dagger}{dt}U_P + U_P^\dagger(\hat{H}_{\text{dia}}(p) + \hat{H}_{\text{off}}(p))U_P$$

$$= \hbar \left\{ \sum_m \widetilde{\Omega}_{k_1,(n,m)} |m+1\rangle\langle m| + \sum_n \widetilde{\Omega}_{k_2,m} |n+1\rangle\langle n| + \sum_{m,n,x,y,i} \widetilde{\Omega_i^{1(2)}} e^{-i[(\omega_{1(2)}^+ - \omega_{2(1)i}^-) - \Delta E_y/\hbar]t + i\widetilde{\phi}_i^{1(2)}} |y+1\rangle\langle y| \right.$$

$$\left. + \sum_{m,n,x,y} \widetilde{\Omega}_{12} e^{-i[\omega_{12}^+ - \Delta E_x/\hbar]t + i\widetilde{\phi}_{12}} |x+1\rangle\langle x| + \sum_{m,n,x,y} \sum_{i,i'} \frac{\Omega_{1i}^-\Omega_{2i'}^-}{4\Delta} e^{i\widetilde{\phi}_{i,i'}} e^{-i[(\omega_{1i}^- - \omega_{2i'}^-) - \Delta E_x/\hbar]t} |x+1\rangle\langle x| + \text{H.c} \right\}. \tag{A17}$$

where

$$\widetilde{\Omega}_{k_1,(n,m)} = \sum_{n,x,y} \sum_i \widetilde{\Omega}_{1i} e^{i\widetilde{\phi}_{1i}} e^{-i[(\omega_1^+ - \omega_{1i}^-) - (E_{m+1} - E_m)/\hbar]t}, \tag{A18}$$

$$\widetilde{\Omega}_{k_2,m} = \sum_{m,x,y} \sum_i \widetilde{\Omega}_{2i} e^{i\widetilde{\phi}_{2i}} e^{-i[(\omega_2^+ - \omega_{2i}^-) - (E_{n+1} - E_n)/\hbar]t} \tag{A19}$$

are the hopping amplitudes between adjacent momentum states $m \to m+1$ and $n \to n+1$. The first two terms satisfy Bragg resonance conditions $[w_1^+ - w_{1i}^- = (E_{m,n} - E_{m+1,n})/\hbar$ and $w_2^+ - w_{2i}^- = (E_{m,n} - E_{m,n+1})/\hbar]$. The last three off-resonant terms are rapidly oscillating with time, and can thus be neglected using a rotating wave approximation. Therefore, the two-leg-coupled SSH model in the main text is achieved.

Acknowledgements

References

[1] Von Klitzing K, Dorda G and Pepper M 1980 *Phys. Rev. Lett.* **45** 494
[2] Thouless D J, Kohmoto M, Nightingale M P and Dennijs M 1982 *Phys. Rev. Lett.* **49** 405
[3] Simon B 1983 *Phys. Rev. Lett.* **51** 2167
[4] Hasan M Z and Kane C L 2010 *Rev. Mod. Phys.* **82** 3045
[5] Qi X L and Zhang S C 2011 *Rev. Mod. Phys.* **83** 1057
[6] Chiu C K, Teo J C Y, Schnyder A P and Ryu S 2016 *Rev. Mod. Phys.* **88** 035005
[7] Bernevig B A and Hughes T L *Topological Insulators and Topological Superconductors* (Princeton: Princeton University Press)
[8] Bansil A, Lin H and Das T 2016 *Rev. Mod. Phys.* **88** 021004
[9] Armitage N P, Mele E J and Vishwanath A 2018 *Rev. Mod. Phys.* **90** 015001
[10] Bzdušek T, Wu Q, Rüegg A, Sigrist M and Soluyanov A A 2016 *Nature* **538** 75
[11] Wang Z, Sun Y, Chen X Q, Franchini C, Xu G, Weng H, Dai X and Fang Z 2012 *Phys. Rev. B* **85** 195320
[12] Burkov A A, Hook M D and Balents L 2011 *Phys. Rev. B* **84** 235126
[13] Benalcazar W A, Bernevig B A and Hughes T L 2017 *Science* **357** 61
[14] Benalcazar W A, Bernevig B A and Hughes T L 2017 *Phys. Rev. B* **96** 245115
[15] Schindler F, Cook A M, Vergniory M G, Wang Z, Parkin S S P, Bernevig B A and Neupert T 2018 *Sci. Adv.* **4** eaat0346
[16] Prodan E, Hughes T L and Bernevig B A 2010 *Phys. Rev. Lett.* **105** 115501
[17] Mondragon-Shem I, Hughes T L, Song J and Prodan E 2014 *Phys. Rev. Lett.* **113** 046802
[18] Yang Y B, Li K, Duan L M and Xu Y 2021 *Phys. Rev. B* **103** 085408
[19] Yao S and Wang Z 2018 *Phys. Rev. Lett.* **121** 086803
[20] Yao S, Song F and Wang Z 2018 *Phys. Rev. Lett.* **121** 136802
[21] Zhang K, Yang Z S and Fang Chen 2020 *Phys. Rev. Lett.* **125** 126402
[22] Okuma N, Kawabata K, Shiozaki K and Sato M 2020 *Phys. Rev. Lett.* **124** 086801
[23] Goldman N, Satija I, Nikolic P, Bermudez A, MartinDelgado M A, Lewenstein M and Spielman I B 2010 *Phys. Rev. Lett.* **105** 255302
[24] Jotzu G, Messer M, Desbuquois R, Lebrat M, Uehlinger T, Greif D and Esslinger T 2014 *Nature* **515** 7526
[25] Junemann J, Piga A, Ran S J, Lewenstein M, Rizzi M and Bermudez A 2017 *Phys. Rev. X* **7** 031057
[26] Konig M, Wiedmann S, Brune C, *et al.* 2007 *Science* **318** 5851
[27] Ueda K, Fujioka J, Takahashi Y, *et al.* 2012 *Phys. Rev. Lett.* **109** 136402
[28] Xie B Y, Wang H F, Wang H X, Zhu X Y, Jiang J H, Lu M H and Chen Y F 2018 *Phys. Rev. B* **98** 205147
[29] Mittal S, Orre V V, Zhu G, Gorlach M A, Poddubny A and Hafezi M 2019 *Nat. Photon.* **13** 692
[30] Ni X, Weiner M, Alù A and Khanikaev A B 2019 *Nat. Mater.* **18** 113
[31] Wei Q, Zhang X, Deng W, Lu J, Huang X, Yan M, Chen G, Liu Z and Jia S 2021 *Nat. Mater.* **20** 812
[32] Yang Z Z, Chen J H, Peng Y Y, *et al.* 2020 *Chin. Phys. B* **29** 104302
[33] Pei D L, Yang T, Chen M, *et al.* 2019 *Chin. Phys. B* **28** 124301
[34] Guo B, Shi K G, Qin H L, *et al.* 2020 *Chin. Phys. B* **29** 097403
[35] Roushan P, Neill C, Chen Y, Kolodrubetz M, *et al.* 2014 *Nature* **515** 241
[36] Cai W, Han J, Mei F, *et al.* 2019 *Phys. Rev. Lett.* **123** 080501
[37] Wang D W, Liu R B, Zhu S Y and Scully M O 2015 *Phys. Rev. Lett.* **114** 043602
[38] Gadway B 2015 *Phys. Rev. A* **92** 043606
[39] Chen L, Wang P, Meng Z, Huang L, Cai H, Wang D W, Zhu S Y and Zhang J 2018 *Phys. Rev. Lett.* **120** 193601
[40] Cai H, Liu J, Wu J, He Y, Zhu S Y, Zhang J X and Wang D W 2019 *Phys. Rev. Lett.* **122** 023601
[41] He Y Y, Mao R S, Cai H, Zhang J X, Li Y Q, Yuan L Q, Zhu S Y and Wang D W 2021 *Phys. Rev. Lett.* **126** 103601
[42] Scully M O, Fry E S, Ooi C H and Wdkiewicz K 2006 *Phys. Rev. Lett.* **96** 010501
[43] An Fangzhao Alex, Meier E J and Gadway Bryce 2017 *Sci. Adv.* **3** e1602685
[44] Meier E J, *et al.* 2018 *Science* **362** 929
[45] Xie D, Gou W, Xiao T, *et al.* 2019 *npj Quantum Inf.* **5** 55
[46] Li L, Umer M and Gong J 2018 *Phys. Rev. B* **98** 205422
[47] Li C, Li S, Zhang G and Song Z 2017 *Phys. Rev. B* **96** 125418
[48] Zhang S L and Zhou Q 2017 *Phys. Rev. A* **95** 061601(R)
[49] Maffei Maria, *et al.* 2018 *New J. Phys.* **20** 013023
[50] Cardano F, *et al.* 2017 *Nat. Comm.* **8** 15516